Light-Induced Second-Harmonic Generation in Glass via Multiphoton Ionization

Vince Dominic* and Jack Feinberg

Departments of Electrical Engineering and Physics, University of Southern California, Los Angeles, California 90089-0484

(Received 1 July 1993)

Irradiating glass by intense light at frequencies ω and 2ω generates a semipermanent dc electric field in the glass that transforms the glass into a phase-matched optical-frequency doubler. We map out this dc electric field over a wide variety of experimental conditions. We show that its symmetries are predicted by a theory based on the interference of competing multiphoton ionization channels.

PACS numbers: 32.80.Fb, 32.80.Rm, 42.65.Ky, 42.70.Ce

Intense light containing frequencies ω and 2ω can produce a semipermanent, spatially periodic dc electric field in glass [1–4]. This strong dc field ($\sim 10^4$ V/cm) then enables phase-matched second-harmonic generation in the glass [5]. A fundamental question is: What microscopic mechanism produces this strong dc electric field? Explanations invoke either light-induced currents [6–8] or structural orientation [5,9]. Our data support the former; the intense light beams at frequency ω and 2ω cause electrons to be ejected with an angular distribution that is not inversion symmetric and which varies periodically in space [10–12]. In this Letter we map out the actual dc electric fields and show, in four different cases, that these fields are well described by a theory based on the interference of different multiphoton ionization channels.

We produce the dc electric field by irradiating a 4 mm thick glass sample (Schott SK-5) with the fundamental ($\lambda = 1.064$ μm) and the second-harmonic light beams of a Q-switched, mode-locked Nd:YAG laser. The peak powers of the infrared and green beam are typically 2 and 0.02 MW, respectively. Both colors are focused to the same spot (to within 0.5 μm) either in the bulk or on the surface of the glass by a lens ($f = 25$ mm) designed to be achromatic at our two wavelengths. After several minutes of intense laser irradiation we block the two seeding beams; any charges that moved during laser irradiation are then trapped in place in the glass. We probe the glass sample with a strongly focused infrared beam and detect any second-harmonic light produced by the glass sample. By inducing the dc field on the surface of the glass and probing with a tightly focused infrared beam we significantly improve the spatial resolution of the dc field maps compared to our previous work [4].

The strength of the generated second-harmonic optical field passing through a polarization analyzer $\hat{\mathbf{e}}_a$ is

$$E_{2\omega} \propto \hat{\mathbf{e}}_a^* \cdot \{\chi^{(3)}_{xyyx}(\hat{\mathbf{e}}_\omega \cdot \hat{\mathbf{e}}_\omega)\hat{\mathbf{e}}_{\mathrm{dc}} + 2\chi^{(3)}_{xxyy}\hat{\mathbf{e}}_\omega(\hat{\mathbf{e}}_\omega \cdot \hat{\mathbf{e}}_{\mathrm{dc}})\} E_{\mathrm{dc}} E_\omega E_\omega , \quad (1)$$

where the circumflex denotes the (possibly complex) unit polarization vector, and E_{dc} and E_ω represent the complex amplitudes of the dc electric field and the infrared optical probing field, respectively. By prudently choosing the reading polarization and the analyzer polarization we can map out the individual components of the dc electric field.

We created four different dc electric field patterns by irradiating separate regions of the glass sample with differently polarized green and infrared seeding beams, as follows: (1) Both seeding beams were $\hat{\mathbf{y}}$ polarized; (2) the infrared beam was $\hat{\mathbf{y}}$ polarized and the green beam was $\hat{\mathbf{x}}$ polarized; (3) the infrared and green seeding beams had the same circular polarization; and (4) the infrared and green seeding beams had opposite circular polarizations.

Figure 1 shows maps of the measured second-harmonic power for case 1. With a $\hat{\mathbf{y}}$-polarized probing beam and a $\hat{\mathbf{y}}$-polarized analyzer we measure the $\hat{\mathbf{y}}$ component of the

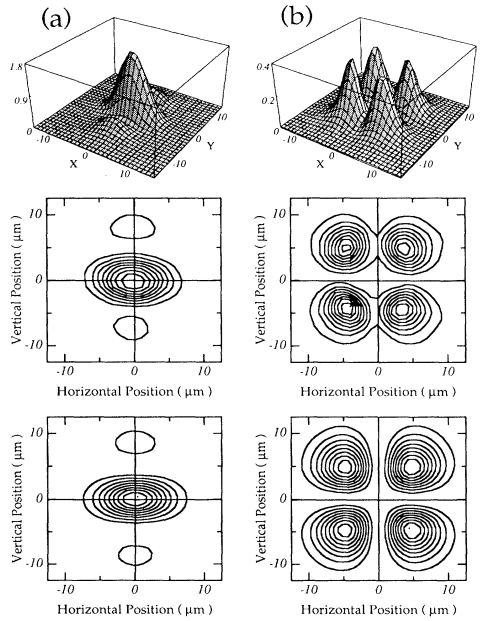

FIG. 1. Strength of the second-harmonic signal versus transverse position after case 1 seeding (see text): (a) $|(E_{\mathrm{dc}})_y|^2$ and (b) $|(E_{\mathrm{dc}})_x|^2$. The top two rows are the experimental data displayed in two formats. The bottom row is calculated from a charge distribution that is the spatial derivative of a Gaussian along the y direction.

0031-9007/93/71(21)/3446(4)$06.00

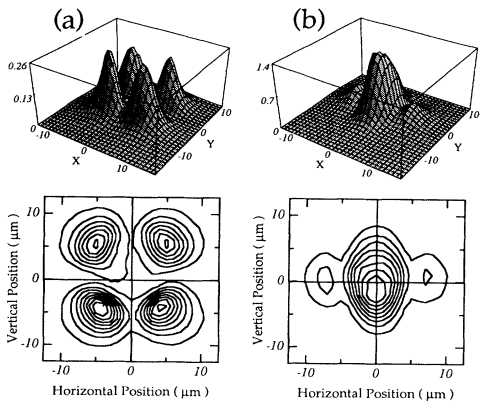

FIG. 2. Strength of the second-harmonic signal versus transverse position after case 2 seeding (see text): (a) $|(E_{dc})_y|^2$ and (b) $|(E_{dc})_x|^2$. The data are identical to that in Fig. 1 except that x and y are now switched, as predicted by theory.

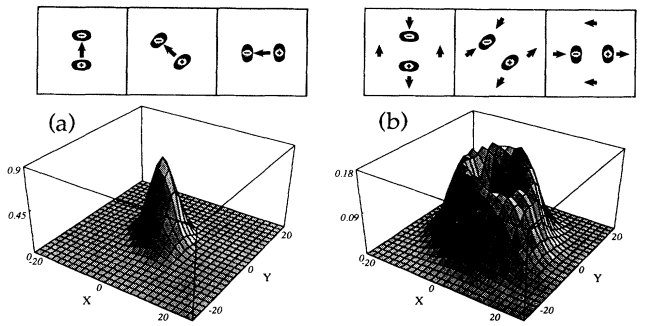

FIG. 3. Strength of the second-harmonic signal versus transverse position after case 3 seeding (see text): (a) $|E_{dc}|^2_{counterclock}$ and (b) $|E_{dc}|^2_{clock}$. The insets show one-quarter period of a spiraling charge pattern and the associated spiraling dc fields. Case (a) picks out any *counterclockwise* spiraling dc field, which is strongest at the center of the spiraling charge pattern. Case (b) picks out any *clockwise* spiraling dc field, which is strongest at the perimeter of the spiraling charge pattern.

dc electric field, $(E_{dc})_y$. Figure 1(a) shows the magnitude $|(E_{dc})_y|^2$ in the x-y plane: We find a strong central hill, with two smaller hills positioned vertically above and below, and the signal decreases to nearly zero between the hills. For Fig. 1(b) we measured the variation of the $\hat{\mathbf{x}}$ component of the dc field, $(E_{dc})_x$, using a probing beam and analyzer that were both $\hat{\mathbf{x}}$ polarized. Now we find four strong peaks, with the signal weak in the interconnecting valleys. The central peak in Fig. 1(a) is a factor of 3 larger than the strongest of the four peaks in Fig. 1(b). These patterns are consistent with charges that had separated along the $\hat{\mathbf{y}}$ direction in the glass, creating a dipolelike electric field [4]. Predicted maps using this *ad hoc* field are shown for comparison.

In case 2 the two seeding beams have different polarizations; the infrared seeding beam is $\hat{\mathbf{y}}$ polarized while the green seeding beam is $\hat{\mathbf{x}}$ polarized. Figure 2 shows that the light-induced dc electric field is now oriented primarily along the $\hat{\mathbf{x}}$ direction; i.e., the charges have migrated along the polarization direction of the incident green beam.

In case 3 we use right circularly polarized infrared and green seeding beams. Now we expect a helical dc field pattern, as sketched in the inset of Fig. 3. The direction of the dc electric field rotates one full turn after traveling in the z direction by the phase-matching periodicity distance $(0.532\ \mu m)/(n_{2\omega}-n_{\omega})=36\ \mu m$, where the n's are the refractive indices at 2ω and ω. Inspection of Eq. (1) shows that the combination right-circular probing beam and right-circular polarization analyzer projects out the spatially counterclockwise-spiraling component of the dc field. Figure 3(a) shows the resulting spatial map: a compact, solitary bump in the center. A left/left probing experiment detects any clockwise-spiraling dc field, and the resulting spatial map [Fig. 3(b)] resembles a volcano. These maps are expected for a spatially spiraling charge distribution, because its dc field rotates in one direction at the center but rotates in the opposite direction off center (see insets). [The signal does not drop completely to zero at the center of Fig. 3(b) due to the finite size of our probing beam.] We confirmed the signal contours shown in all the above figures with numerical calculations that account for the spatial shape of the dc electric field and the propagation of the Gaussian probing beams [4].

Finally, we prepared the sample with seeding beams having opposite circular polarizations (case 4), and measured a peak signal strength that was 400 times weaker than the peak signal strengths in cases 1–3 above, and with a dc field that spiraled in the opposite direction than the dc field in case 3. However, the purity of our circular polarizations was only ~95%, and any leakage of the opposite circular polarization of the green beam would produce the mirror image of case 3.

We also performed separate experiments to confirm the orientation of the dc electric field. We position the probing beam at each pattern's center of symmetry, rotate both the probing beam's linear polarization and the linear analyzer to an angle Φ, and measure the signal strength as a function of Φ. Figure 4 shows our measurements plotted in cylindrical coordinates, where the radial distance is the strength of the measured second-harmonic signal. The solid lines are fits using Eq. (1), assuming that the dc electric field at the center is purely in the $\hat{\mathbf{y}}$ direction for case 1 [Fig. 4(a)] and purely in the $\hat{\mathbf{x}}$ direction for case 2 [Fig. 4(b)]. The fit for case 3 [Fig. 4(c)] allows the Cartesian components of the dc electric field to be spatially out of phase (as expected for a spiraling field), so that the maximum of the $\hat{\mathbf{x}}$ component of the field occurs at a different z plane than the maximum of the $\hat{\mathbf{y}}$ component. The fit gave a ratio of $(E_{dc})_y/(E_{dc})_x = 1.1 \pm 0.2$ (instead of the expected 1) and a spatial

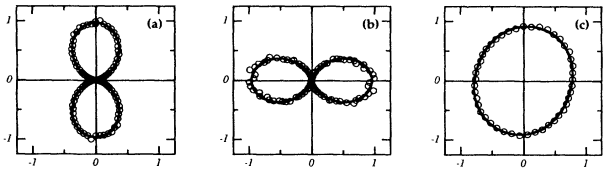

FIG. 4. Polar maps of the measured (circles) and predicted (solid lines) dc electric field strength at the center of Figs. 1, 2, and 3. (a) In case 1 the field is completely along $\hat{\mathbf{y}}$. (b) In case 2 the field is completely along $\hat{\mathbf{x}}$. (c) In case 3 the dc field spirals with z.

phase shift between the field components of $87.2° \pm 1.5°$ (instead of the expected 90°).

These spatial maps, as well as the far-field maps of Dianov *et al.* [3], convincingly rule out structural orientation models since these models predict signals that monotonically decrease with distance from the beam center. In contrast, we observe spatial structure in the measured signal consistent with a dc electric field produced by charge separation.

Photogalvanic current models [6,7] predict a dc current $\mathbf{j}_{pg}$ proportional to [13]

$$\mathbf{j}_{pg} \propto \{a(\hat{\mathbf{e}}_\omega^* \cdot \hat{\mathbf{e}}_\omega^*)\hat{\mathbf{e}}_{2\omega} + 2b\hat{\mathbf{e}}_\omega^*(\hat{\mathbf{e}}_\omega^* \cdot \hat{\mathbf{e}}_{2\omega})\} E_\omega^* E_\omega^* E_{2\omega} \exp(i\Delta kz) , \quad (2)$$

where $\Delta k = k_{2\omega} - 2k_\omega$. Equation (2) contains the distinct combinations of vectors in an isotropic media that give another vector which uses all three of the optical fields $E_\omega \hat{\mathbf{e}}_\omega$, $E_\omega \hat{\mathbf{e}}_\omega$, and $E_{2\omega}\hat{\mathbf{e}}_{2\omega}$ precisely once and that varies as $\exp(i\Delta kz)$. The dc electric field arising from this current possesses all of the symmetries of our data. However, this form of $\mathbf{j}_{pg}$ lacks many of the details contained in richer, more complete theories. We expand the multiphoton ionization model [8] here and show that the polarization dependences of Eq. (2) are recovered. We assume that electrons in the glass are ejected after absorbing either a single green photon or two infrared photons, and that these two ionization channels interfere. In fact, the number of absorbed photons is larger than this in glass [14]. However, our experiments here probe only the $\exp(i\Delta kz)$ component of the charge distribution, in fact, only its transverse symmetries, and this phase-matched component is always produced by the interference of channels having one unmatched green photon and two unmatched infrared photons. We have also derived the expected photoelectron angular distributions for cases having additional photons [15] and find that, even when we include the proliferation of possible angular momentum states, we obtain the same transverse symmetries.

For simplicity we assume an s-type ground state, nonresonant ionization, the dipole approximation, classical fields, hydrogenic intermediate state wave functions, and no spin-orbit coupling. We make the standard partial-wave expansion of the electron wave-function final state

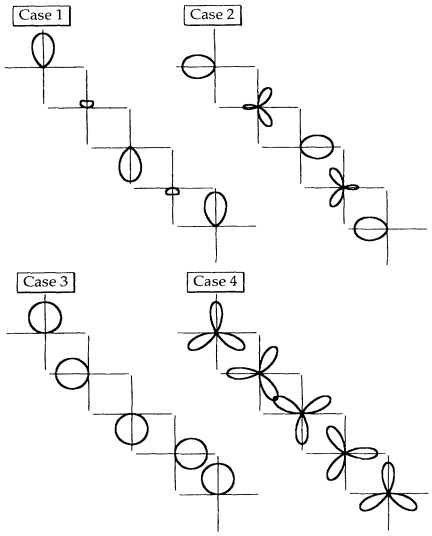

FIG. 5. Plots of the probability for ejecting electrons in the x-y plane at different z planes for cases 1 through 4 above. The charges are asymmetrically ejected primarily along $\hat{\mathbf{y}}$ for case 1, $\hat{\mathbf{x}}$ for case 2, in a spiral for case 3, and in a spiral of opposite handedness for case 4.

[16]. We let z be the propagation direction and the optical polarization vectors lie in the x-y plane. The continuum state can be reached by *either* of two ionization paths, and in these experiments we cannot distinguish which path was taken. Consequently, the two paths interfere to produce the following angular distribution:

$$\frac{d\sigma}{d\Omega} \propto |M_{fi}^{(1)} + M_{fi}^{(2)}|^2 , \quad (3)$$

where $M_{fi}^{(1)}$ and $M_{fi}^{(2)}$ are the one- and two-photon matrix elements, respectively. The cross terms in the expansion of Eq. (3) vary periodically along the propagation direction z. These terms are not inversion symmetric; they eject the electrons in a preferred direction, and create the spatially periodic, transverse, dc electric field.

Figure 5 shows plots of the probability of electron ejection vs azimuthal angle Φ for the four different cases. If the infrared and the green beams are both $\hat{\mathbf{y}}$ polarized (case 1), then in the plane transverse to the propagation direction the noncentrosymmetric term in the angular distribution is

$$\left.\frac{d\sigma}{d\Omega}\right|_{\text{noncentro}} = \{Q + Q' \sin^2\Phi\}\{Q'' \sin\Phi\} \exp(i\Delta kz) + \text{c.c.} , \quad (4)$$

where the bracketed terms arise from two- and one-photon ionization, respectively. The complex Q's include the radial overlap integral, the summation over intermediate states, and the scattering phase shift. In Eq. (4) the preferential direction of electron ejection is seen to

vary sinusoidally with z between $+\hat{\mathbf{y}}$ and $-\hat{\mathbf{y}}$ (because of the $\sin\Phi$ term in the second bracket) in agreement with our data. That is, the charges separate along the y direction, creating a dipole field. Case 1 was also studied in Refs. [2–4,11,12,17] and their data are consistent with the simple analysis given here.

For case 2, where the infrared light is $\hat{\mathbf{y}}$ polarized but the green light is $\hat{\mathbf{x}}$ polarized, theory gives a result identical to Eq. (4) but with $\cos\Phi$ substituted for $\sin\Phi$ in the second bracketed term. In agreement with our data, the preferential direction of electron ejection has now switched to vary periodically between $+\hat{\mathbf{x}}$ and $-\hat{\mathbf{x}}$.

For case 3, where both the green and the infrared are right circularly polarized, we find

$$\left.\frac{d\sigma}{d\Omega}\right|_{\text{noncentro}} = \{Q''' e^{i\Phi}\} \exp(i\Delta k z) + \text{c.c.} \tag{5}$$

Now the preferential direction of electron ejection rotates in the x-y plane periodically with z, and so produces a helical dc field. Our theory predicts that this helical field spirals with the same spatial handedness as the green circular polarization (so long as we are in a normally dispersive wavelength range, where $n_{2\omega} - n_{\omega} > 0$), and this is what we observe.

Finally, if the infrared is right and the green is left circularly polarized we obtain

$$\left.\frac{d\sigma}{d\Omega}\right|_{\text{noncentro}} = \{Q''' e^{i3\Phi}\} \exp(i\Delta k z) + \text{c.c.} \tag{6}$$

Now the electron ejection pattern has become three lobed and spirals in the opposite direction from case 3. This three-lobed ejection pattern is inefficient in producing an electric field in the x-y plane (and, in fact, produces a zero electric field at the center). The dc field is expected to be small in this case, as we observe.

In conclusion, we find excellent agreement between the predictions of photocurrent models and the measured spatial shapes of the dc electric field induced in glass samples by intense light beams at frequencies ω and 2ω. Our data rule out structural reorientation models. The symmetries contained in the photocurrent model can be derived from the interference of two multiphoton ionization channels. We also note the universality of the symmetries observed here; we found similar dc electric field shapes in all the glass samples that we tried to date, including a GeO_2-doped SiO_2 optical fiber preform, and samples of Schott Glass SK4 and BK7.

We thank Dan Elliott for informative and pleasant discussions, and Joseph Haydn of Schott Glass and Frank Dabby of Ensign-Bickford Optical Technologies, Inc. for glass samples. This work was supported by AFOSR Grant No. F49620-92-J-0022.

Note added.—Since the submission of this manuscript we have learned of similar measurements [17] that confirm our cases 1 and 2.

*Present address: Electro-Optics Program, University of Dayton, 300 College Park, Dayton, OH 45469-0227.

[1] A. Kamal *et al.*, in *Digest of Optical Society of America Annual Meeting* (Optical Society of America, Washington, DC, 1990), paper PD25.
[2] V. Mizrahi, Y. Hibino, and G. Stegeman, Opt. Commun. **78**, 283 (1990).
[3] E. M. Dianov, P. G. Kazansky, D. S. Starodubov, and D. Yu. Stepanov, Sov. Lightwave Commun. **2**, 83 (1992).
[4] V. Dominic and J. Feinberg, Opt. Lett. **18**, 784 (1993).
[5] R. H. Stolen and H. W. K. Tom, Opt. Lett. **12**, 585 (1987).
[6] E. M. Dianov, P. G. Kazansky, and D. Yu. Stepanov, Kvant. Elektron. (Moscow) **16**, 887 (1989) [Sov. J. Quantum Electron. **19**, 575 (1990)].
[7] B. Ya. Zel'dovich and A. N. Chudinov, Pis'ma Zh. Eksp. Teor. Fiz. **50**, 405 (1989) [JETP Lett. **50**, 439 (1989)].
[8] D. Z. Anderson, V. Mizrahi, and J. E. Sipe, Opt. Lett. **16**, 796 (1991).
[9] F. Charra, F. Kajzar, J. M. Nunzi, P. Raimond, and E. Idiart, Opt. Lett. **18**, 941 (1993).
[10] H. G. Muller, P. H. Bucksbaum, D. W. Schumacher, and A. Zavriyev, J. Phys. B **23**, 2761 (1990).
[11] N. B. Baranova, I. M. Beterov, B. Ya. Zel'dovich, I. I. Ryabtsev, A. N. Chudinov, and A. A. Shul'ginov, Pis'ma Zh. Eksp. Teor. Fiz. **55**, 451 (1992) [JETP Lett. **55**, 439 (1992)].
[12] Y.-Y. Yin, C. Chen, D. S. Elliott, and A. V. Smith, Phys. Rev. Lett. **69**, 2353 (1992).
[13] E. M. Dianov, V. O. Sokolov, and V. B. Sulimov, Sov. Lightwave Commun. **2**, 133 (1992).
[14] V. Dominic and J. Feinberg, Opt. Lett. **17**, 1761 (1992).
[15] V. Dominic, Ph.D. thesis, University of Southern California, 1993.
[16] S. J. Smith and G. Leuchs, in *Advances in Atomic and Molecular Physics* (Academic, Boston, 1988), Vol. 24.
[17] M. A. Bolshtyansky, V. M. Churikov, Yu. E. Kapitzky, A. Yu. Savchenko, and B. Ya. Zel'dovich, Pure Appl. Opt. **1**, 289 (1992).